Gas Phase and Aqueous Thermochemistry of Hydrazine and Related Radicals and the Energy Profiles of Reactions with H• and OH•: An ab Initio Study

D. A. Armstrong,* D. Yu, and A. Rauk*

Department of Chemistry, The University of Calgary, Calgary, Alberta, Canada T2N 1N4

Received: December 12, 1996; In Final Form: April 1, 1997[⊗]

Ab initio calculations by a modified G2(MP2) procedure have been used to obtain bond dissociation energies, proton affinities, and heats of formation of hydrazine (H_2NNH_2) and the related radicals and radical ions. Bond dissociation energies and proton affinities in these species are strongly influenced by the three-electron stabilization, which occurs in $HNNH_2^{\bullet}$ and $H_2NNH_2^{\bullet+}$. Free energies of formation in solution were estimated and used to examine relative stabilities of the radicals and the overall energetics of their reactions. For example, $H_2NNH_2^{\bullet+}$ is 100 kJ mol^{-1} more stable than $HNNH_3^{\bullet+}$, and this explains the rearrangement which has been observed experimentally. As a guide to the relative importance of possible reactions, the energy profiles of the reactions of H_2NNH_2 and $H_2NNH_3^+$ with H• and OH• in the gas phase were also studied. With H_2NNH_2, barrier heights above reactants are generally low for the H abstraction reactions of both OH• (−5 kJ mol^{-1}) and H• (25 kJ mol^{-1}), which is consistent with the low activation energies observed experimentally. For $H_2NNH_3^+$, reaction profiles for attack at both the H_2N and NH_3^+ sites were examined. In the case of OH•, abstraction of H from the $-NH_3^+$ end to form $H_2NNH_2^{\bullet+}$ is preferred over production of $HNNH_3^{\bullet+}$ by attack at H_2N-. However, in solution the former mode will be inhibited by the strong bonding of water to the charged NH_3^+ end, and attack at both centers can be expected. For H• attack on $H_2NNH_3^+$, formation of $H_2NNH_2^{\bullet+}$ by H abstraction from the NH_3^+ end has a very low gas phase E_a, but in solution solvation effects will again interfere. Thus production of $H_3NNH_3^{\bullet+}$ by H addition at H_2N is likely to be a competitive process. This product is expected to decompose to $H_2N^{\bullet} + NH_4^+$ ($\Delta G^\circ_{(react)} = -13$ kJ mol^{-1}), and complexation of water with $H_3NNH_3^{\bullet+}$ was shown to lower the barrier height for that process. In the gas phase prereaction complexes of OH• are seen with both H_2NNH_2 and $H_2NNH_3^+$, the latter being quite strongly bound. However, competition with solvent water molecules would probably reduce the role of these in solution.

Introduction

Hydrazine is used as a rocket fuel and as a corrosion inhibitor for steel structures in contact with hot water.[1,2] These uses arise from the fact that it is an endothermic compound ($\Delta_f H^\circ_{298} =$ 95.4 kJ mol^{-1} [3]) and reaction 1 is exothermic by 580 kJ mol^{-1}.[4]

$$N_2H_4(g) + O_2(g) = N_2(g) + H_2O(g) \qquad (1)$$

N_2H_4 (**1**) is a bifunctional base with p$K_a = -1$ for $H_3NNH_3^{2+}$ and 8.0 for $H_2NNH_3^+$ (**2**).[4] The main forms in aqueous systems at pH 7 are therefore **1** and **2**. The $H_2NNH_3^+$ species has recently been found to be a very effective corrosion inhibitor in the aqueous systems of nuclear reactors.[1,2] Under irradiation conditions, the principal radical species produced are the solvated electron, $e_{(aq)}^-$, and hydroxyl radical, OH•, in roughly equal numbers and smaller amounts of H• atom.[5] It is important to note that the reaction of $e_{(aq)}^-$ with $H_2NNH_3^+$, reaction 2, produces predominantly H• atoms.[2] Therefore, in hydrazinium solutions the reactions of H• become as important as OH•.

$$e_{(aq)}^- + H_2NNH_3^+ = H_2NNH_2 + H^{\bullet}; \quad \Delta G^\circ_{(Rxn)} = -10 \text{ kJ mol}^{-1} \qquad (2)$$

The H• and OH• radicals are considered to react with the hydrazine species to form $HNNH_2^{\bullet}$ (**3**), $H_2NNH_2^{\bullet+}$ (**4**), and $HNNH_3^{\bullet+}$ (**5**).[6−10] The species $H_3NNH_3^{\bullet+}$ (**6**) has been postulated to exist in low-temperature crystals,[11] but there is no information on its role in liquid water. Obviously knowledge of the properties of all of these hydrazinium radicals is very important. We have therefore carried out an investigation of the structures and thermochemical properties of radicals **3**−**6** by ab initio methods. Free energies of formation in solution and free energies of reaction of several radical reactions were estimated. Also the energy profiles for the reactions of OH• and H• with N_2H_4 (**1**) and $H_2NNH_3^+$ (**2**) were investigated in the gas phase as a means of estimating the relative heights of the barriers to different reactions.

Methods

Computational Details. All ab initio calculations presented here were performed with the Gaussian-94 molecular orbital packages.[12] For all the species under study, the total energies were effectively estimated at the G2(MP2) level.[13] The G2-(MP2) procedure normally includes zero-point vibrational energy (ZPE) corrections at the HF/6-31G(D) level (scaled by 0.8929), a step which requires prior geometry optimization at the same level, and geometry reoptimization at the MP2/6-31G-(D) level. Because for many radical systems the Hartree−Fock geometry is significantly different from that obtained by correlated procedures (MP2, B3LYP) and because the 6-31G-(D) basis set is also somewhat limiting for processes involving hydrogen transfers and bonding, we have determined the geometries and vibrational frequencies at the B3LYP/6-31+G-(D,P) level.[14] This procedure normally produces reliable geometries and energies but, as discussed below, may be problematic in some cases involving transition states. The vibrational frequencies calculated at the B3LYP/6-31+G(D,P) level were scaled by a factor of 0.95 in considering the zero-point energy.[15] The remaining steps in the G2(MP2) prescrip-

* Authors to whom correspondence should be addressed.

[⊗] Abstract published in *Advance ACS Abstracts,* June 1, 1997.

S1089-5639(96)04057-1 CCC: $14.00

TABLE 1: Ideal Gas Thermodynamic Properties at 298 K[a]

	C_P°, J K^{-1} mol^{-1}	S°, J K^{-1} mol^{-1}	$H^\circ - H_0^\circ$, [b] kJ mol^{-1}	$\Delta_f H^\circ$, kJ mol^{-1}	$\Delta_f G^\circ$, kJ mol^{-1}
$NH_2^\bullet$	33.6	194.7	9.9	**188.7**[c] **(191.6)**[c]	199
$NH_3^{\bullet+}$	36.5	193.1	10.1	936.8 **(943.7)**[d]	966
NH_3	35.5	192.6	10.1	**−46.1 (−39.1)**	**−16.5**
NH_4^+	34.9	185.9	10.0	**631.4**[e] (642.7)	682
1 NH_2-NH_2	47.3;**49.6**	230.7;**238.5**	11.1;**11.5**	**95.4 (109.5)**	**159.4**
2 $NH_2-NH_3^+$	48.4	240.8	11.5	761 (779)	844
3 $NH-NH_2^\bullet$	44.9	238.1	11.0	225 (235)	270
4 $NH_2-NH_2^{\bullet+}$	53.9	242.5	12.4	877 (891)	940
5 $NH-NH_3^{\bullet+}$	48.0	248.4	11.9	996 (1009)	1057
6 $NH_3-NH_3^{\bullet+}$	76.0	276.0	15.9	749 (767)	842

[a] Values in bold face are experimental values from ref 3 or as stated. Values for 0 K are in parentheses. [b] For H_2, 8.5 kJ mol^{-1}; for N_2, 8.7 kJ mol^{-1}. [c] From ref 28. [d] From IP in ref 28 and ΔH_0° of NH_3. [e] PA from ref 20.

tion are intended to provide an accurate description of corrections for higher order correlation and larger basis sets and were adopted as originally described, namely two single-point post-HF calculations, QCISD(T)/6-311G(D,P) and MP2/6-311+G-(3DF,2P) (at the B3LYP/6-31+G(D,P) geometry except as noted), and a "high-level correction" factor. In spite of the minor modification, we will refer to this level as "G2(MP2)", bearing in mind that the energies of some of the species will not be identical to other published values because of the slight difference in the geometry and ZPE term.

Transition structures for the H abstraction reactions of $H^\bullet$ and $OH^\bullet$ with H_2N-NH_2 (**1**) and for seven reactions of $H^\bullet$ and $OH^\bullet$ with $H_2N-NH_3^+$ (**2**) were located.

Thermodynamic Properties. For the equilibrium structures under study, the ideal gas thermodynamic functions C_P°, S°, and $H^\circ - H_0^\circ$ at 298.15 K and at 1 bar were calculated by standard statistical thermodynamic methods based on the rigid rotor−harmonic oscillator model.[16] The vibrational frequencies calculated at the B3LYP/6-31+G(D,P) level were scaled by a factor of 0.95 in such calculations.[15] The $H^\circ - H_0^\circ$ data were used for all species where procedures used gave $\Delta_f H^\circ$ values at only one temperature. The values of S° and $H^\circ - H_0^\circ$ for the reference elements are taken from Wagman, et al.[3]

Although reasonably accurate values of $\Delta_f H^\circ$ could be calculated directly by the G2(MP2) procedure,[17] the accuracy can be improved by the use of isodesmic reactions.[18,19] Since the proton affinity (853 kJ mol^{-1} at 298 K[20]) and bond dissociation energy of ammonia (446.4 kJ mol^{-1} at 0 K[21]) are well known, as are the heats of formation of relevant ammonia species, the following two reactions were used in the present instance:

$$N_2H_x + NH_4^+ = N_2H_{x+1}^+ + NH_3 \quad (3)$$

$$N_2H_x + NH_2^\bullet = N_2H_{x-1}^\bullet + NH_3 \quad (4)$$

Reaction 3 involves a proton transfer and makes use of the experimental PA of ammonia. It may be used directly to calculate the proton affinity (PA) of the hydrazine species or $\Delta_f H^\circ$ of one of the species, provided the $\Delta_f H^\circ$ of the other is accurately known. Reaction 4 involves a hydrogen atom transfer and makes use of the experimental bond dissociation energy (BDE) of ammonia. It may be used directly to calculate the BDE of the hydrazine species or $\Delta_f H^\circ$ of one of the species, again provided the $\Delta_f H^\circ$ of the other is accurately known. The specific process used for each hydrazine species is explained below. A suitable isodesmic reaction could not be found for $H_3NNH_3^{\bullet+}$ (**6**). However, $\Delta H_{(Rx)}^\circ$ for reaction (5),

$$H_3NNH_3^{\bullet+} = H_3N + NH_3^{\bullet+} \quad (5)$$

was derived from the G2(MP2) results, and $\Delta_f H^\circ$ of **6** was determined from that and the experimental $\Delta_f H^\circ$s for H_3N and $NH_3^{\bullet+}$.

The isodesmic reaction method is expected to reduce errors in $\Delta_f H^\circ$ to <10 kJ mol^{-1}. Values were taken from the isodesmic reactions or from the experimental literature, if they existed and were supported by the isodesmic results. For ions, $\Delta_f H^\circ$s were calculated in accord with the "ion convention".[22] Free energies of formation, $\Delta_f G^\circ$, were obtained from the values of $\Delta_f H^\circ$ in conjunction with the theoretical entropy data.

Results and Discussion

Selected structural features of the optimized geometries at the B3LYP/6-31+G(D,P) level are presented in Figures 1−4, which also display reaction profiles. Species **1**, **2**, and **6** appear as reactants in Figures 1a, 2, and 4a, respectively. Other species appear as products: **3** in Figure 1b, **4**, **5**, and **7** in Figure 2. The ZPEs and the total energies of these species are listed in Table S1 of the Supporting Information. Thermodynamic properties are listed in Tables 1 and 2.

Equilibrium Structures. All structures correspond to minima on the potential energy surfaces as verified by vibrational frequency calculations. Except for $HN-NH_2^\bullet$ (**3**), the optimized species have symmetries higher than C_1 (C_s for $H_2N-NH_3^+$ (**2**) and $HN-NH_3^{\bullet+}$ (**5**), C_{2h} for $H_2N-NH_2^{\bullet+}$ (**4**), C_2 for H_2N-NH_2 (**1**), and D_{3d} for $H_3N-NH_3^{\bullet+}$ (**6**)). The geometry of H_2N-NH_2 (**1**) is similar to that found in earlier theoretical studies[23,24] and in good agreement with experiment.[25] The N−N bonds of the π radicals, $HN-NH_2^\bullet$ (**3**, 1.352 Å) and $H_2N-NH_2^{\bullet+}$ (**4**, 1.318 Å), are shorter by about 10% than those of H_2N-NH_2 (**1**), $H_2N-NH_3^+$ (**2**), and $HN-NH_3^{\bullet+}$ (**5**) due to participation of the $-NH_2$ lone pair in three-electron π bonding. An additional consequence of this is that both species are quasi-planar. In particular, for $H_2N-NH_2^{\bullet+}$ (**4**), this represents a substantial geometry change from the parent hydrazine **1** which has a perpendicular orientation of the nonbonded electron pairs. On the other hand, three-electron σ bonding in $H_3N-NH_3^{\bullet+}$ (**6**) results in a substantially longer N−N bond (2.151 Å).[26] The structure of $H_2N-OH^{\bullet+}$ (**7**), which is a potential product of $OH^\bullet + H_2NNH_3^+$, is planar with C_s symmetry, Figure 2.

Thermodynamic Properties. C_P°, S°, and $H^\circ - H_0^\circ$. The values of these thermodynamic functions calculated from the ab initio frequencies are given for all species in Table 1. Experimental data are only available for the parent, H_2NNH_2 (**1**). The agreement between the calculated and experimental values, which are in bold face in the table, is excellent. Comparable accuracy is expected for C_P°, S°, and $H^\circ - H_0^\circ$ computed for the other compounds.

$\Delta_f H^\circ$. Table 1 contains the values of $\Delta_f H^\circ$ for the hydrazine-derived species and all ammonia-derived species used in the isodesmic reactions. Experimental data (given in bold face in the table) exist for all of the ammonia species and for the parent hydrazine (**1**). Therefore, all $\Delta_f H^\circ$ values reported here for **2**−**6** are with reference to those for H_2NNH_2 at 0 and 298 K.[3] $\Delta_f H^\circ$ of **2**, **3**, and **4** *may* be derived from experimental determinations of the PA, N−H BDE, and ionization potential (IP), respectively,

SCHEME 1

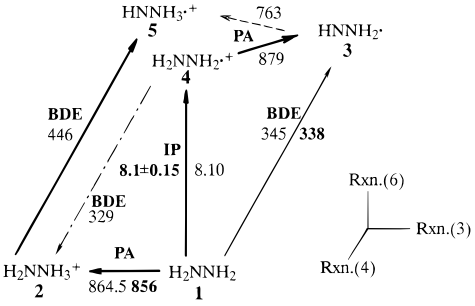

for **1**. However, these are subject to relatively large uncertainties and are examined in detail below.

The steps employed in obtaining heats of formation are explained in Scheme 1. Vertical, horizontal, and diagonal directions correspond to the use of reactions 6, 3, and 4, respectively.

$$H_2NNH_2 + NH_3^{\bullet+} = H_2NNH_2^{\bullet+} + NH_3 \qquad (6)$$

The directions of the heavy arrows indicate the path used to obtain the heat of formation for each hydrazine species from the H_2NNH_2 parent. The directions of light and dashed arrows are secondary routes. IPs in eV, and BDEs and PAs in kJ mol^{-1} are given on connecting arrows with experimental values in bold face. The PAs are at 298 K since they are only available from experiment at this temperature. All other data are at 0 K. Apart from their relevance to the $\Delta_fH°$ values, the IP, BDE, and PA data are of intrinsic interest. They are therefore discussed in separate sections after discussion of the $\Delta_fH°$ and $\Delta_fG°$ results.

$\Delta_fH°$ of Hydrazine (1). The experimental values, $\Delta_fH°_0 =$ 109.5 kJ mol^{-1} and $\Delta_fH°_{298} = 95.4$ kJ mol^{-1}, were adopted and serve as the reference for all other heats of formation derived in the next sections. The experimental uncertainty is less than 1 kJ mol^{-1}.[3]

$\Delta_fH°$ of the Parent Ion $H_2N-NH_2^{\bullet+}$ (4). The heat of formation of $H_2N-NH_2^{\bullet+}$ (**4**) could be derived directly from the experimental IP of **1**, but this is subject to a rather large uncertainty (±14 kJ mol^{-1}). A more accurate value (effectively for the IP of **1**, see below) may be derived from the calculated heat of reaction 6 (−201.1 ± 2 kJ mol^{-1} at 0 K), making use of the accurately known experimental IP of NH_3 (982.84 ± 0.01 kJ mol^{-1})[27] and $\Delta_fH°_0$ of **1**. The value thus obtained for **4** is $\Delta_fH°_0 =$ 891 ± 2 kJ mol^{-1}, from which one may derive $\Delta H°_{298} =$ 877 ± 2 kJ mol^{-1}.

$\Delta_fH°$ of $H_2N-NH_3^+$ (2). The heat of formation of $H_2N-NH_3^+$ (**2**) at 298 K may be derived from the heat of reaction 3 (−12.0 kJ mol^{-1}), $\Delta_fH°_{298}$ of **1**, and the PA of ammonia. The value thus obtained for **2** is $\Delta_fH°_{298} = 760.9$ kJ mol^{-1}, from which may be derived $\Delta_fH°_0 = 779$ kJ mol^{-1}. The dot-dashed arrow of Scheme 1 indicates a second path to $\Delta_fH°_0$ of **2** through the isodesmic reaction 7:

$$H_2NNH_3^+ + NH_2^{\bullet} = H_2NNH_2^{\bullet+} + NH_3 \qquad (7)$$

The result thus obtained, 778 kJ mol^{-1}, agrees well with $\Delta_fH°_0$, indicating internal consistency in the results.

$\Delta_fH°$ of $HN-NH_2^{\bullet}$ (3). The heat of formation of $HN-NH_2^{\bullet}$ (**3**) at 0 K may be calculated from the heat of reaction 4 (−101.6 kJ mol^{-1}), the BDE of ammonia, and $\Delta_fH°_0$ of **1**. This gave directly for **3** $\Delta_fH°_0 = 238.3$ kJ mol^{-1}, and therefore, $\Delta_fH°_{298} =$ 228.4 kJ mol^{-1}. The calculated value of $\Delta_fH°_0$ is in fair agreement with the experimental value, 231.4 kJ mol^{-1},[28] but the difference is larger than expected. Reaction 3, making use of $\Delta_fH°_{298}$ of **4** and the PA of ammonia, provides an independent value for $\Delta_fH°_{298}$ of **3**, 226.6 kJ mol^{-1}, and subsequently, $\Delta_fH°_0 = 237.8$ kJ mol^{-1}. The 0 and 298 K results are close to those derived via reaction 4. We therefore average the theoretical (reaction 4) and experimental 0 K values and adopt for **3** $\Delta_fH°_0 = 235$ kJ mol^{-1}, from which is derived $\Delta_fH°_{298} =$ 225 kJ mol^{-1} (Table 1).

TABLE 2: Free Energies of Formation and Solution (kJ mol^{-1})

species	$\Delta_fG°$(g)	$\Delta G°$(soln)	$\Delta_fG°$(aq)
H$^{\bullet}$	218[b]	3.0	221[c]
NH_3	−16.5[b]	−10.0[b]	−26.5[b]
$NH_2^{\bullet}$	199[d]	−8.0[d]	191[d]
$NH_3^{\bullet+}$	966	729	178
NH_4^+	682	756	−79.3[b]
OH$^{\bullet}$	34[b]	−8	26[e]
H_2O	−228.6	−18.4	−247.0
1 H_2NNH_2	159.4[b]	−31.3[b]	128.1[b]
2 $H_2NNH_3^+$	844	756	82.5[b]
3 $HNNH_2^{\bullet}$	270	−31	239
4 $H_2NNH_2^{\bullet+}$	940	775[f]	198[f]
5 $HNNH_3^{\bullet+}$	1057	756	296
6 $H_3NNH_3^{\bullet+}$	842	800	125

[a] From this study unless otherwise indicated. Standard states are 1 bar gas, 1 M in solution. [b] Experimental from ref 3. [c] From ref 40. [d] From ref 34. [e] Experimental value from ref 41. [f] $\Delta_fG°$(aq) and $\Delta G°$(soln) calculated from $\Delta_fG°$(aq) of **3** and the experimental pK_a of **4** from ref 2.

$\Delta_fH°$ of $HN-NH_3^{\bullet+}$ (5). The heat of formation of $HN-NH_3^{\bullet+}$ (**5**) at 0 K was calculated from the heat of reaction 4 (−0.3 kJ mol^{-1}), the BDE of ammonia, and $\Delta_fH°_0$ of **2**. The value thus obtained for **5** is $\Delta_fH°_0 =$ 1009 kJ mol^{-1}, and subsequently, $\Delta_fH°_{298} =$ 996 kJ mol^{-1}.

$\Delta_fH°$ of $H_3N-NH_3^{\bullet+}$ (6). A suitable isodesmic reaction could not be found for $H_3NNH_3^{\bullet+}$ (**6**). However, the heat of reaction **5** was derived from the G2(MP2) results and used together with the experimental $\Delta_fH°$s for H_3N and $NH_3^{\bullet+}$ to obtain for **6** $\Delta_fH°_0 = 767$ kJ mol^{-1}, from which is derived $\Delta_fH°_{298} = 749$ kJ mol^{-1} (Table 1). These values will have a greater uncertainty, approximately 10 kJ mol^{-1}, than the other heats of formation reported here.

$\Delta_fG°$(aq) and $\Delta G°$(soln). Table 2 summarizes the aqueous solution data. The convention of setting $\Delta_fG°$(aq) of $H^+ =$ 0.000 has been followed.[3] This means that for positive ions:

$$\Delta_fG°(\text{aq}) = \Delta G°(\text{soln}) + \Delta_fG°(\text{g}) - \Delta_fG°(\text{g}) \text{ of } H^+ \qquad (8)$$

where

$$\Delta G°(\text{soln}) = \Delta G°(\text{soln} - \text{absolute}) - \Delta G°(\text{soln} - \text{absolute}) \text{ of } H^+ \qquad (9)$$

The recommended value of $\Delta G°$(soln − absolute) of H^+ is −1079 kJ mol^{-1},[29] and for the ion convention used here, $\Delta_fG°$(g) of $H^+ =$ 1517 kJ mol^{-1}.[30] $\Delta_fG°$(aq) for H_2NNH_2 (**1**) and $H_2NNH_3^+$ (**2**) were taken from ref 3. $\Delta G°$(soln) for these species was found from those values and the values of $\Delta_fG°$(g) in Table 1, which are repeated in column two of Table 2 for ease of reference. The $\Delta G°$(soln) values for hydrazinium radicals were estimated in most cases from the parent species of similar structures, e.g. $\Delta G°$(soln) for $HNNH_2^{\bullet}$ (**3**) and $HN-NH_3^{\bullet+}$ (**5**) are taken to be the same as those of H_2NNH_2 (**1**) and $H_2NNH_3^+$ (**2**), respectively. $\Delta_fG°$(aq) was then calculated from the $\Delta G°$(soln) and the $\Delta_fG°$(g). However, $\Delta_fG°$(aq) of $H_2N-NH_2^{\bullet+}$ (**4**) was found from its experimental pK_a[2] and $\Delta_fG°$(aq) of $HNNH_2^{\bullet}$ (**3**). Also, in accord with the Born theory of ion solvation, $\Delta G°$(soln) of $H_3NNH_3^{\bullet+}$ (**6**) was increased above that of **2** in proportion to the increase in van der Waals radius obtained from the ab initio structures. The uncertainty

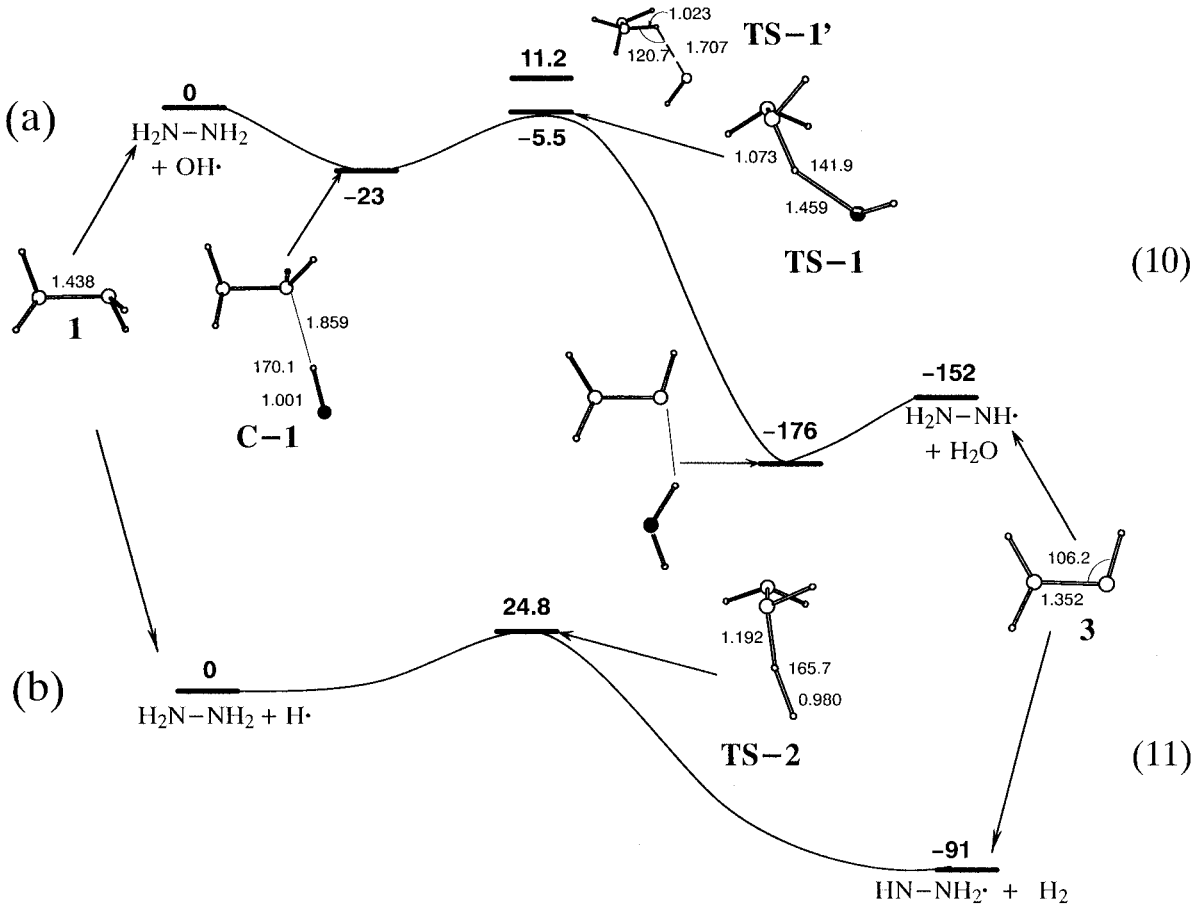

Figure 1. Reactions of H_2N-NH_2 (**1**) with H• and OH•: reaction profiles at the G2(MP2) level and the optimized structures at the B3LYP6-31+G(D,P) level with characteristic parameters. The large circles stand for nitrogen and the small circles represent the hydrogen atoms. The filled circles stand for oxygen. Bond lengths are in angstroms and angles in degrees. The numbers are the relative energies in kJ mol^{-1}.

in the $\Delta_f G°$(aq) values for the radicals is ±15 kJ mol^{-1}, except for $H_3N-NH_3^{\bullet+}$ where it is ±20 kJ mol^{-1}.

Ionization Potentials (IPs) and Proton Affinities (PAs). *IP*. The tabulated experimental adiabatic IP of hydrazine (**1**) is 8.1 ± 0.15 eV.[22] The relatively large uncertainty probably reflects the experimental difficulties caused by the significant difference in the structures of H_2N-NH_2 (**1**) and $H_2N-NH_2^{\bullet+}$ (**4**) (see Figures 1 and 2). The IP derived from the G2(MP2) energies of H_2N-NH_2 and $H_2N-NH_2^{\bullet+}$ is 8.11 eV, in agreement with the G2 value, 8.09 eV.[31] The value from the isodesmic reaction 6 was 8.10 eV. On the basis of the uncertainties in the heat of the isodesmic reaction and the IP of ammonia noted above, the IP of hydrazine can be set at 8.10 ± 0.02 eV.

PAs. The PA of H_2N-NH_2 (**1**) at 298 K from isodesmic reaction 3 was 864.5 kJ mol^{-1}. The direct G2(MP2) value was 862 kJ mol^{-1}. These are both in fair agreement with experiment (856 kJ mol^{-1} [3]). Since ab initio calculations give accurate PAs in general and because the PA of NH_3 is well established,[20] we have used the 864.5 kJ mol^{-1} value to calculate $\Delta_f H° = 761$ kJ mol^{-1} at 298 K for $H_2N-NH_3^+$ (**2**). For $HN-NH_2^{\bullet}$ (**3**) the PAs at 298 K from reaction 3 are 879 kJ mol^{-1} at the dicoordinated nitrogen (the radical center) and 763 kJ mol^{-1} at the other nitrogen. Therefore, compared to hydrazine **1**, removal of one H somewhat increases the basicity at the radical center, but substantially reduces it at the other N atom.

BDEs. *N−H BDEs*. Application of isodesmic reaction 4 yields $D_{N-H} = 345$ kJ mol^{-1} for H_2N-NH_2 (**1**) at 0 K. The G2(MP2) energies of H_2N-NH_2 (**1**) and $HN-NH_2^{\bullet}$ (**3**) directly yield $D_{N-H} = 342.3$ kJ mol^{-1} (343.5 kJ mol^{-1} at the G2 level[31]). All of the theoretical values are within the expected error range of the 0 K experimental value, 338 kJ mol^{-1}.[28] The N−H BDE of hydrazine is substantially lower than that of ammonia (446 kJ mol^{-1} at 0 K[21]), an observation which is attributable to the preferential stabilization of the product radical **3** by three-electron bonding.

The 0 K N−H BDEs of $H_2N-NH_3^+$ (**2**) derived from H transfer reaction 4 are 446 and 329 kJ mol^{-1} for the $-NH_2$ group and the $-NH_3^+$ group, respectively. Thus the BDE at the protonated site is similar to that in H_2NNH_2 (**1**), again illustrating the effect of the adjacent lone pair in stabilizing the product radical **4**. No such stabilization is possible at the unprotonated site and D_{N-H} is predicted to be essentially the same as that of ammonia. The difference in the two BDEs of **2** is, of course, also the difference in the $\Delta_f H°$ of the isomeric product radicals $H_2N-NH_2^{\bullet+}$ (**4**) and $HN-NH_3^{\bullet+}$ (**5**). As a matter of curiosity the BDE of N−H in the $H_3N-NH_3^{\bullet+}$ radical (**6**) (230 kJ mol^{-1}) is significantly smaller than that in H_2NNH_2. This very low N−H BDE is due to a combination of unstable starting material (**6** has one too many electrons) and stable product (**2** is a closed shell species).

N−N BDEs. The experimental value of the N−N BDE of H_2N-NH_2 (**1**) has recently been reported to be 274.1 ± 1.7 kJ mol^{-1},[28] which is in accord with the $\Delta_f H_0^\circ$ values for $NH_2^{\bullet}$ and H_2N-NH_2 (**1**) in Table 1. Direct ab initio calculations previously yielded 266.9 kJ mol^{-1} [32] and 267.9 kJ mol^{-1}.[24] The N−N bond in $H_3N-NH_3^{\bullet+}$ (**6**) is very much weaker, 130 kJ mol^{-1} from the present G2(MP2) energies and 137 kJ mol^{-1} from the $\Delta_f H_0^\circ$ values in Table 1. The latter agrees well with 138 kJ mol^{-1} found by Gill and Radom.[26]

Reaction Profiles and Aqueous Reaction Mechanisms. The following subsections relate to the possible reactions of H_2NNH_2 (**1**) and $H_2NNH_3^+$ (**2**) with H• and OH•. For every case the underlying reactions are defined in a figure which also displays the G2(MP2) gas phase reaction profiles, with energies

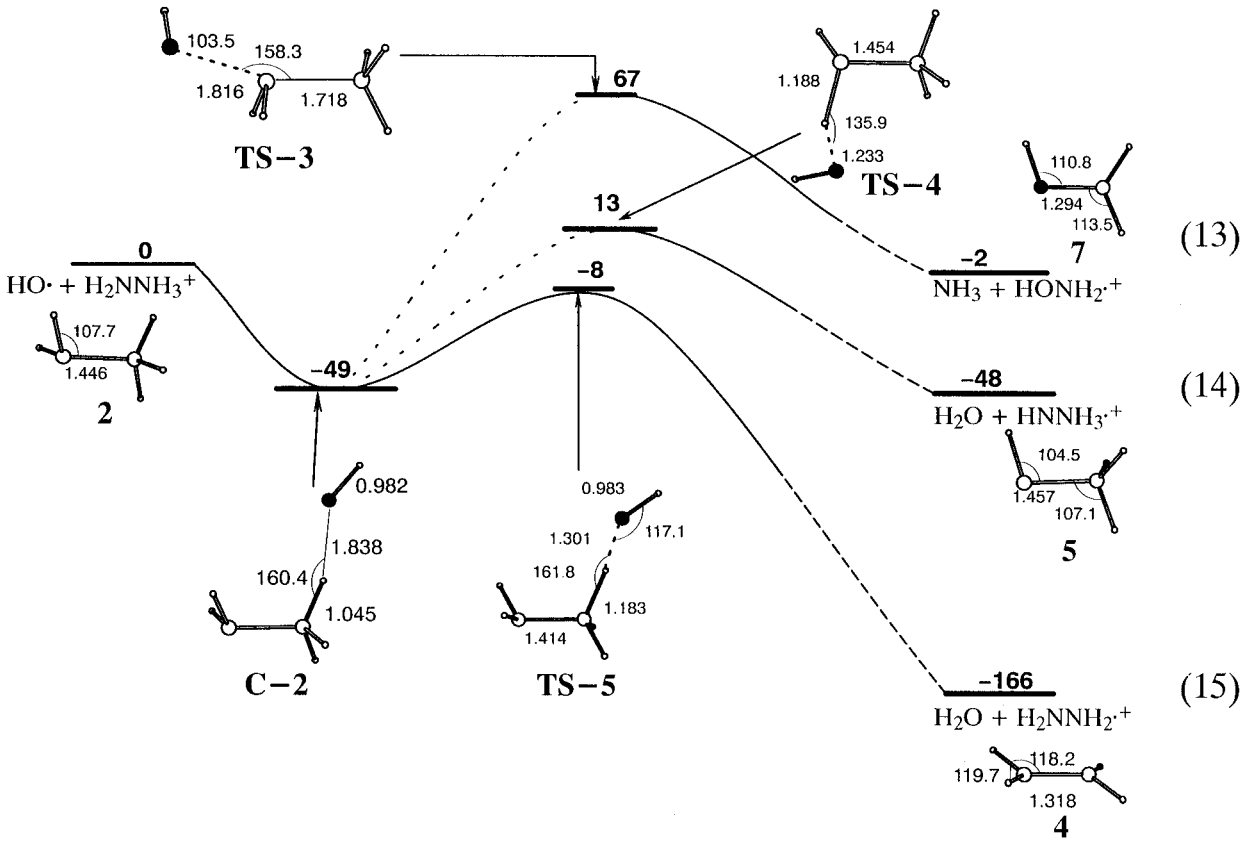

Figure 2. Reactions of $H_2N-NH_3^+$ (**2**) with OH•: symbols as in Figure 1.

of activation and 0 K heats of reaction (in kJ mol^{-1}). The reactions are discussed, and in several cases it was found that certain processes would be uncompetitive and could be eliminated. Possible aqueous solution reactions are then listed in identically numbered equations in the text with the free energies of reaction calculated from the data in Table 2. Specific effects of solution are considered, and the conclusions from theory are compared to available experimental results.

(i) $OH^\bullet + H_2NNH_2$ (**1**)

Gas Phase. Of the possible interactions between the two reactants, $OH^\bullet + H_2NNH_2$ (**1**), the H abstraction in reaction 10 (Figure 1a) was the only process examined. At the B3LYP/6-31+G(D,P) level, a single prereaction complex was found, **C-1**, characterized by an OH···N hydrogen bond. The G2(MP2) energy of **C-1** is lower by 23.0 kJ mol^{-1} than **1** + OH•. While MP2 optimization with the same basis set yielded essentially the same structure as **C-1**, the B3LYP and MP2 potential energy surfaces are radically different in the vicinity of the transition state for hydrogen transfer. No transition state for direct H• abstraction by OH• could be located at the B3LYP/6-31+G-(D,P) level. Any approach by OH• to an *endo* H of hydrazine resulted in H atom loss without activation. A transition structure **TS-1′** (Figure 1a) for *inversion* of the N atom bearing a hydrogen in close proximity (1.707 Å) to the hydroxyl was located at this level, however. The normal mode with the imaginary frequency suggests that N inversion may be accompanied by H atom loss since the separation between the H and O is decreased. However, the N−H distance is hardly elongated. The G2(MP2) energy of **TS-1′** is 11.2 kJ mol^{-1} above the separated species. By contrast, at MP2/6-31+G(D,P) level, **TS-1** (Figure 1a), a well-defined transition structure for H abstraction by OH• was found. **TS-1** is directly connected to the H-bonded complex, **C-1**. The G2(MP2) energy of **TS-1** is 5.5 kJ mol^{-1} *below* the reactants **1** and OH•. In view of the differences between the B3LYP and MP2 results in the vicinity of the transition state, single-point QCISD(T)/6-31+G(D,P) calculations were carried out at selected points along the MP2 intrinsic reaction coordinate on either side of **TS-1**. The results confirm the existence of a transition structure well above **C-1** but below the separated reactants, as shown in Figure 1a. **TS-1** is typical of an early transition state since the N−H bond being broken is elongated by only 7% while the forming H−O bond is 50% longer than its final value in water. The gas phase reaction between OH• and H_2NNH_2 does not appear to have been studied experimentally. It would be interesting to see whether the formation of the complex **C-1** results in a negative activation energy as has been observed in some other cases with similar characteristics.[33]

Solution Phase.

$$OH^\bullet + H_2NNH_2 = HNNH_2^\bullet + H_2O; \quad \Delta G^\circ(\text{Rxn}) = -162 \text{ kJ mol}^{-1} \quad (10)$$

The aqueous phase reaction is exergonic by 162 kJ mol^{-1}, and expected to be fast. Experimentally it has been shown to be partially controlled by diffusion with the k_{react} rate constant having an activation energy of 12 kJ mol^{-1}.[2] This low magnitude is in keeping with the general profile of the reaction in the gas phase, Figure 1a. The role of the prereaction complex **C-1**, if any, appears to be minimal. In that regard it may be noted, based on results for NH_3,[34] that the hydrogen-bonding energy for the association of a N lone pair with HO of H_2O is 20 kJ mol^{-1} and similar to that for **C-1** in Figure 1a. Hence, formation of **C-1** would require OH• to displace H_2O molecules and its significance may be diminished. On the other hand hydrogen bonding for an H_2O lone pair with an H−N bond is quite weak, 4−8 kJ mol^{-1},[34] and formation of the transition state **TS-1** shown in Figure 1a would be less hampered.

(ii) $H^{\bullet} + H_2NNH_2$ (**1**)

Gas Phase. Experimental studies have confirmed that the formation of H_2 and $HNNH_2^{\bullet}$ (**3**), reaction 11 (Figure 1b), is the only important reaction channel for $H^{\bullet} + H_2NNH_2$.[35] As in the case of $OH^{\bullet}$, the B3LYP and MP2 potential energy surfaces for the H abstraction process are radically different. On the B3LYP surface, the reaction proceeds without activation while G2(MP2) energies at selected geometries along the reaction coordinate suggest that there should be a barrier. MP2 optimization yields **TS-2** (Figure 1b) for which the G2(MP2) energy is 24.8 kJ mol^{-1} above the reactants, $H^{\bullet} + H_2NNH_2$ (**1**). Single-point QCISD(T)/6-31+G(D,P) calculations were carried out at selected points along the MP2 intrinsic reaction coordinate on either side of **TS-2**. The higher level calculations confirm that **TS-2** is close to the correct geometry for the hydrogen abstraction transition state. There is no evidence of a prereaction complex. The experimental Arrhenius activation energy over the range 222−657 K is 10.5 ± 0.2 kJ mol^{-1}.[35] On correction to the transition state format[36] this corresponds to 10.2 kJ mol^{-1}, which is substantially smaller than the barrier estimated on the basis of the MP2 TS structure, **TS-2**. The experimental value of the barrier does not take into account rate enhancement due to quantum mechanical tunneling. The Wigner correction for tunneling, κ, is given by[37]

$$\kappa \approx 1 + \frac{1}{24}\left(\frac{h\nu^{\ddagger}}{k_B T}\right)^2 \qquad (11)$$

where $\nu^{\ddagger}$ is the magnitude of the imaginary frequency, 2320*i* cm^{-1}, and k_B is Boltzmann's constant. Application of eq 11 to the low and high end of the experimental temperature range predicts rate enhancements of $\kappa = 10.4$ (222 K) and $\kappa = 2.1$ (657 K), respectively. Thus, corrected for tunneling, the experimental classical Arrhenius activation energy is 14.8 kJ mol^{-1}, in somewhat better agreement with theory.

The reaction is strongly exothermic and passes through a very early transition structure, **TS-2**. As with **TS-1**, one of the *endo* hydrogen atoms is involved. Abstraction of this H is assisted by involvement of the nonbonded electron pair of the other N atom.

Solution Phase.

$$H^{\bullet} + H_2NNH_2 = HNNH_2^{\bullet} + H_2; \quad \Delta G^{\circ}(\mathrm{Rxn}) = -110 \text{ kJ mol}^{-1} \qquad (12)$$

Although the $H_2O\cdots HN$ bonds are weak (see above), the nonpolar $H^{\bullet}$ atom with have more difficulty than $OH^{\bullet}$ in displacing H_2O to form the reaction complex. Experimentally the reaction of $H^{\bullet}$ is slower than that of $OH^{\bullet}$, and diffusion control is not an important factor.[10] The rate constant is described by the equation $k = 4.9 \times 10^{10}(\exp -(16280/RT))$ dm^3 mol^{-1} s^{-1}. The activation energy, 16.3 kJ mol^{-1}, is thus raised somewhat, closer to the calculated gas phase value.

(iii) $OH^{\bullet} + H_2NNH_3^{+}$ (**2**)

Gas Phase. In the case of $H_2NNH_3^{+}$ (**2**) several reaction channels were examined. These are shown in Figure 2. The ion-dipole interaction between $OH^{\bullet}$ and the charged NH_3^{+} is very strong and produces the complex **C-2** 49 kJ mol^{-1} below $OH^{\bullet} + H_2NNH_3^{+}$ (**2**). Reactions 13, 14, and 15 (Figure 2) can therefore be regarded as unimolecular processes starting from the **C-2** structure, and having activation energies of 116, 62, and 41 kJ mol^{-1}, respectively. Each of the products, **4**, **5**, and **7**, forms a strong H-bonded complex with the coproduced water or ammonia, but these are not shown in Figure 2. On the basis of the predicted activation energies, reaction 13 which would produce hydroxylaminium (**7**) via **TS-3** is clearly noncompetitive and there does not appear to be any experimental evidence for it. The alternative displacement reaction 16

SCHEME 2: H_2O−Hydrogen Bonding to $H_2N-NH_3^{+}$ (2).

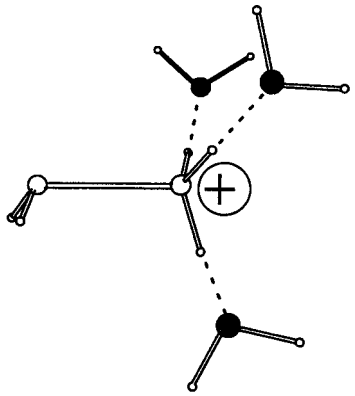

$$OH^{\bullet} + H_2NNH_3^{+} = H_2NOH + NH_3^{\bullet+} \qquad (16)$$

was considered and found to be 80 kJ mol^{-1} endothermic. Both are therefore dismissed from further consideration.

The relative energies of the transition structures for reaction 14 (**TS-4**) and reaction 15 (**TS-5**) are as expected on the basis of the relative N−H BDEs of **2**. Indeed, when one realizes that reaction 15 is more exothermic by ∼120 kJ mol^{-1}, the difference in activation energy seems rather small. It may be rationalized as follows. One can see from Figure 2 that in the TS of reaction 14, **TS-4**, the negative O end of the dipolar $OH^{\bullet}$ is directed toward the positive charge of the $-NH_3$ group. At the same time the singly occupied orbital is properly aligned to accept the H atom. On the other hand in **TS-5**, the TS of reaction 15, the ion dipole interaction causes the $H\cdots O-H$ bond angle to be abnormally large (117°), and this will add to the barrier height. Neither of these reactions appears to have been studied experimentally in the gas phase.

Solution Phase.

$$OH^{\bullet} + H_2NNH_3^{+} = H_2O + HNNH_3^{\bullet+}; \quad \Delta G^{\circ}(\mathrm{Rxn}) = -60 \text{ kJ mol}^{-1} \qquad (14)$$

$$OH^{\bullet} + H_2NNH_3^{+} = H_2O + H_2NNH_2^{\bullet+}; \quad \Delta G^{\circ}(\mathrm{Rxn}) = -158 \text{ kJ mol}^{-1} \qquad (15)$$

Both reactions are clearly exergonic, and the obvious gas phase preference for reaction 15 may be altered in solution by the strong binding of H_2O molecules to the positively charged NH_3^{+} end of the $H_2NNH_3^{+}$ reactant, see Scheme 2. From experimental[38] and theoretical[39] studies on NH_4^{+} and by direct calculation (B3LYP/6-31+G(D,P)) on $\mathbf{2}\cdots(H_2O)_3$ (Scheme 2), the average binding energy of water in the first layer can be expected to be about 70 kJ mol^{-1}, and $OH^{\bullet}$ would have to compete for access to the H atoms of the positively charged $-NH_3$ end. The neutral NH_2 is further away from the charge center, and H_2O around it would be more weakly bound and more easily displaced. Thus, from the point of view of dynamics, the obvious preference for formation of **TS-5**, the transition state for reaction 15, in the gas phase should be reduced, and the pathway for forming $HNNH_3^{\bullet+}$ (**5**), i.e. reaction 14, could even become preferred.

The above effect can explain the observed formation of significant amounts of $HNNH_3^{\bullet+}$ (**5**) in aqueous solution.[2]

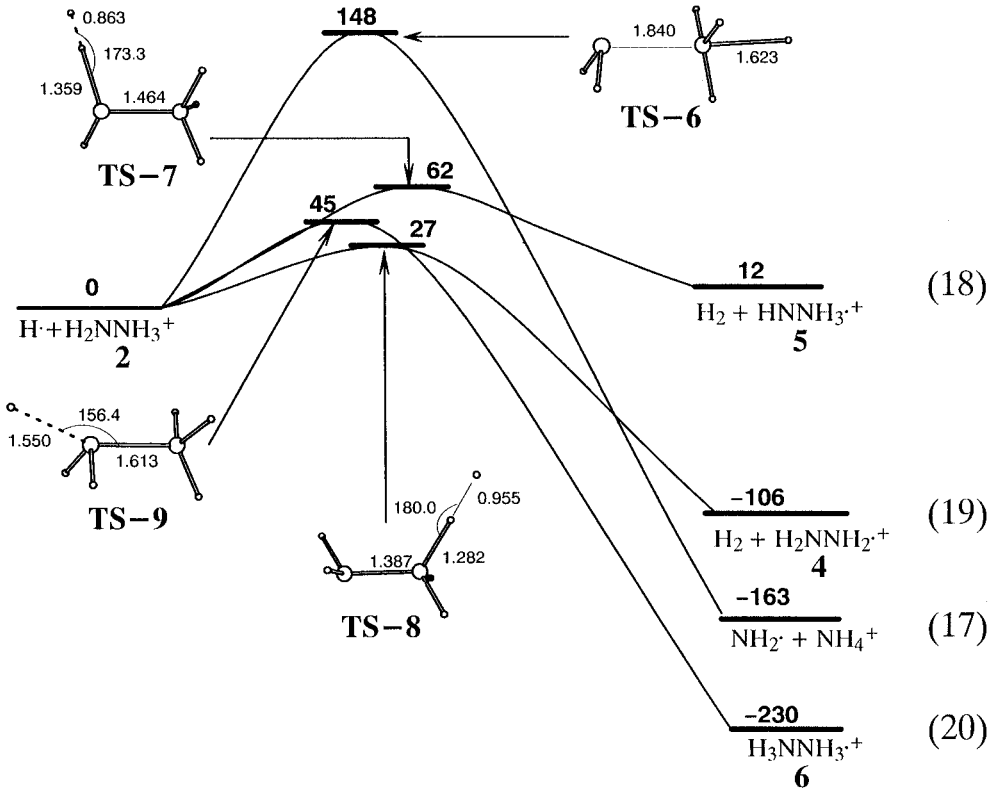

Figure 3. Reactions of $H_2N-NH_3^+$ (**2**) with H•: symbols as in Figure 1.

However, **5** was seen to rearrange to $H_2NNH_2^{\bullet+}$ (**4**) on a microsecond time scale. This is expected based on the fact that $\Delta_f G°$(aq) of **4** is about 100 kJ mol^{-1} more negative than that of $HNNH_3^{\bullet+}$ (**5**) (Table 2).

It may be noted that the overall rate constant for reaction of OH• with $N_2H_5^+$ in water is $(8.2 \pm 1.2) \times 10^7$ dm^{-3} mol^{-1} s^{-1}.[2] The activation energy is apparently $\lesssim$5 kJ mol^{-1}.[2] That would be in keeping with a diminished effect of the prereaction complex. However, the reaction is relatively slow, and appears to have a significant negative $\Delta S°$(Rxn). It is obviously a complex process, which requires further investigation.

(iv) $H^\bullet + H_2NNH_3^+$ (**2**)

Gas Phase. Several reaction channels were again examined, and the results are displayed in Figure 3. No significant prereaction complex was detected. The activation energy of reaction 17, via **TS-6** in which the H atom approaches the N atom of the $-NH_3$ group, causes its inversion, and displaces the $H_2N^\bullet$ radical, is 148 kJ mol^{-1}. It is much larger than those of the others, and it clearly cannot compete. Reaction 18, which involves H abstraction from the neutral end of **2**, is 12 kJ mol^{-1} endothermic in the gas phase and has an activation energy, via **TS-7**, of 62 kJ mol^{-1}. The energy of **TS-7** is much higher than the transition structures of reactions 19 (**TS-8**, 27 kJ mol^{-1}) and 20 (**TS-9**, 45 kJ mol^{-1}) (Figure 3). Reactions 17 and 18 are not, therefore, considered further.

Solution Phase.

$$H^\bullet + H_2NNH_3^+ = H_2 + H_2NNH_2^{\bullet+};$$
$$\Delta G°(\text{Rxn}) = -106 \text{ kJ mol}^{-1} \quad (19)$$

$$H^\bullet + H_2NNH_3^+ = H_3NNH_3^{\bullet+};$$
$$\Delta G°(\text{Rxn}) = -179 \text{ kJ mol}^{-1} \quad (20)$$

Clearly reaction 19 is kinetically the most favorable H• reaction in the gas phase, with reaction 20 second. However, as discussed in relation to OH• and Scheme 2 above, in solution the formation of **TS-8** for reaction 19 will be inhibited by the $H_2O\cdots H-N$ hydrogen bonds around the protonated end of $N_2H_5^+$ (**2**). It may be noted that this effect would be even stronger for H• than for OH•, since the large dipole moment of OH• would allow it to displace H_2O more easily than the nonpolar H•. This may make it possible for reaction 20 to compete with 19 in solution and play a significant role.

The rate of H• atom attack on $N_2H_5^+$ has been found from experiment to be relatively slow. The 298 K rate constant is 1.2×10^6 dm^{-3} mol^{-1} s^{-1},[10] considerably slower than for the reaction of OH•. The activation energy has been estimated to be 61 kJ mol^{-1}, and there is a large positive entropy of activation. Mezyk et al.[10] point out that this is incompatible with H abstraction (reaction 19). They suggest it could be accounted for by an initial step involving hydrogen atom addition followed by a breakdown to form $NH_2^\bullet$, NH_3 and H^+. This would be consistent with the observation that $NH_2^\bullet$ and NH_4^+ are main products from the attack of H• on $N_2H_5^+$ in water at neutral pH and that H_2 production from reaction 19 is much less important.[2] The energy profile for the breakdown of $H_3NNH_3^{\bullet+}$ (**6**) to form $NH_2^\bullet$ and NH_4^+ is examined in the next section. Here one may note that the experimental $\Delta S^\ddagger$ of 71 J K^{-1} mol^{-1} for the $H^\bullet + N_2H_5^+$ reaction could be explained by reaction 20, if $S°$ of **TS-9** in solution is $\sim$260 J K^{-1} mol^{-1}. This is based on solution $S°$ values of 151 and 42 J K^{-1} mol^{-1} for $H_2NNH_3^+$ and H. $S°$ of **TS-9** would definitely be greater than that of $H_3NNH_3^{\bullet+}$, which in the gas phase is 276 J K^{-1} mol^{-1} (Table 1). The experimental activation energy, 61 kJ mol^{-1}, is too high to be associated with reaction 19 and more comparable to the 45 kJ mol^{-1} barrier for reaction 20. The origin of this lies in the stretching of the N−N bond.

(v) $H_3NNH_3^{\bullet+}$ (**6**) $\rightarrow H_2N^\bullet + NH_4^+$

Gas Phase. Previous work showed that the gas phase activation energy for rearrangement of $H_3NNH_3^{\bullet+}$ (**6**) to $H_2N^\bullet$ and NH_4^+ was about 40 kJ mol^{-1}.[26] It is important to know

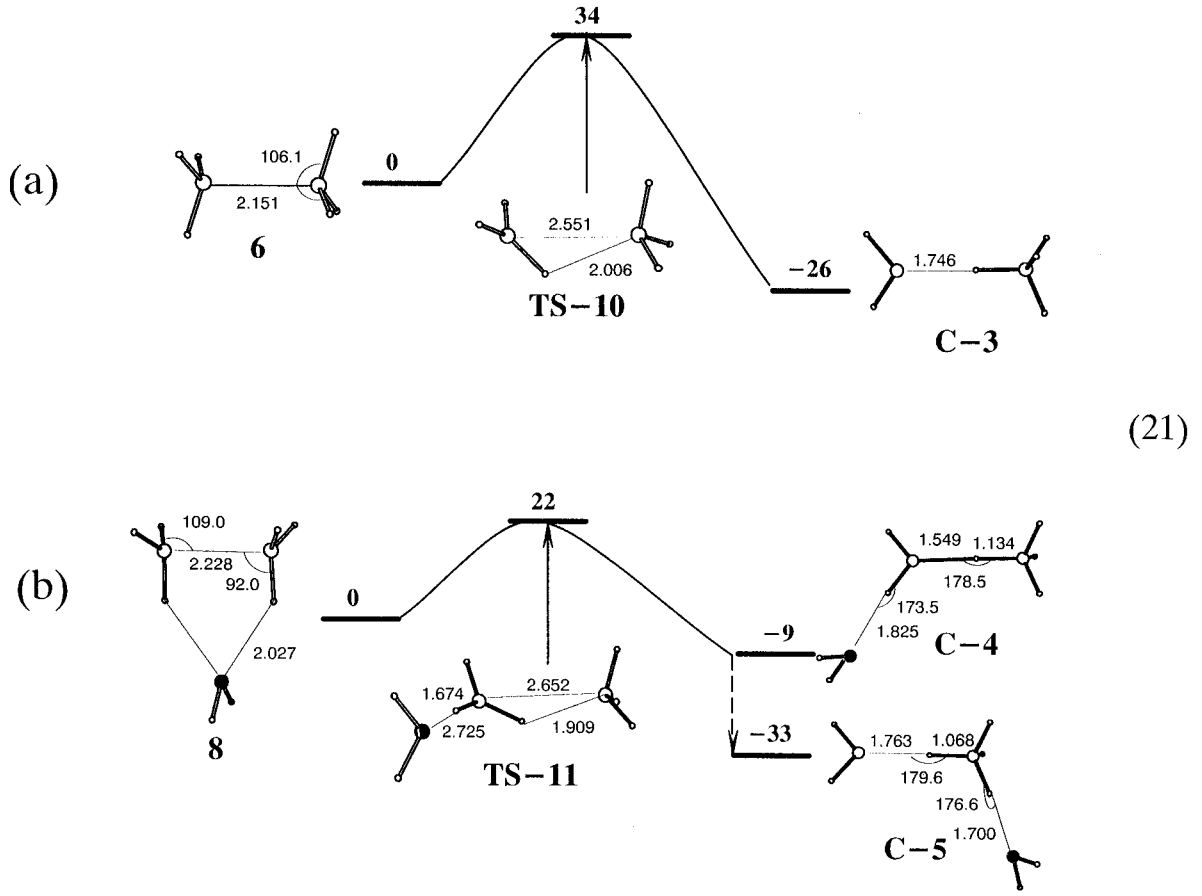

Figure 4. Reaction profiles at the G2(MP2) level and the optimized structures at the B3LYP6-31+G(D,P) level for the decomposition of $H_3NNH_3^{\bullet+}$ (**6**) to $H_2N^{\bullet}$ and NH_4^+, (a) without and (b) with one water of hydration: symbols as in Figure 1.

how this will be influenced by the presence of water. Accordingly, the effect of bound water on the process was investigated. The energy profiles with and without water are shown in Figure 4 (reactions 21: Figure 4a without water, Figure 4b with water).

The gas phase reaction profile without the presence of water (Figure 4a) is essentially the same as that found by Gill and Radom.[26] At G2(MP2) level, the transition structure, **TS-10**, is 34 kJ mol^{-1} above **6** and the reaction is exothermic by 26 kJ mol^{-1} at 0 K. In **TS-10**, the N−N bond of **6** is essentially broken and the transition structure has the characteristic of $NH_3^{\bullet+}$ in the process of transferring a proton to NH_3. The most stable complex between **6** and a single water molecule, structure **8**, has C_{2v} symmetry as shown in Figure 4b with a binding energy of 54 kJ mol^{-1}. Decomposition of the $H_3NNH_3^{\bullet+}$ fragment proceeds through **TS-11** in which the more acidic $NH_3^{\bullet+}$-like end has the hydrogen-bound water molecule. **TS-11** poses a reduced activation barrier to the process: 22 kJ mol^{-1}. The transition states, **TS-10** and **TS-11**, are reached *prior* to the transfer of the proton to form the products $H_2N^{\bullet}$ and NH_4^+ in the form of a hydrogen-bonded complex, **C-3** or **C-4**. Because of the charge distribution in **TS-10**, an attempt to bind a single water molecule to the neutral $-NH_3$ end simply results in its migration to the other end to form **TS-11**. However, the direct product of the reaction, **C-4**, in which the water remains with the (now) $H_2N^{\bullet}$ end of the product complex, is 24 kJ mol^{-1} less stable than the alternative hydrated product complex, **C-5**, in which the water is at the NH_4^+ end. Although we did not attempt to search for structures with two water molecules, it is reasonable to postulate that a second water molecule situated at the NH_3-like end of **TS-11** may further lower the activation energy to reaction 21 since the more stable product complex, akin to **C-5** (Figure 4b) may be formed directly.

Solution Phase.

$$H_3NNH_3^{\bullet+} = H_2N^{\bullet} + NH_4^+; \qquad \Delta G°(\text{Rxn}) = -13 \text{ kJ mol}^{-1} \quad (21)$$

The electron spin resonance spectrum of $H_3NNH_3^{\bullet+}$ has been reported in low-temperature glasses, where it is relatively stable.[11] However, as indicated in the above equation, the $\Delta_f G°$(aq) results in Table 2 suggest that reaction 21 is 13 kJ mol^{-1} exergonic and in solutions at the temperatures of interest (300−500 K) it should proceed at a significant rate if the activation energy is not large. The present results show that the activation energy will be reduced in solution. If one takes a maximum value of 22 kJ mol^{-1} and a normal transition state preexponential factor of 10^{13} s^{-1}, the half-life at 298 K would be $\leq$0.5 ns. At the same time, one cannot eliminate the possibility that stretching of the N−N bond as the H atom approaches in reaction 20 is accompanied by rotation of the NH_3 groups. This might allow a **TS-10**-type transition state to be formed, bypassing $H_3NNH_3^{\bullet+}$ (**6**). A distinction between these two possibilities is beyond the scope of this project. Clearly, an experimental search for $H_3NNH_3^{\bullet+}$ (**6**) at room temperature would be of considerable interest.

The present thermochemical results show that reaction 22 is exergonic by 102 kJ mol^{-1}. Thus $NH_2^{\bullet}$ radicals formed from $e_{(aq)}^-$ via reactions 2, 20, and 21 can oxidize $H_2NNH_3^+$ (**2**) to $H_2NNH_2^{\bullet+}$:

$$NH_2^{\bullet} + H_2NNH_3^+ = NH_3 + H_2NNH_2^{\bullet+}; \qquad \Delta G°(\text{Rxn}) = -102 \text{ kJ mol}^{-1} \quad (22)$$

However, the reaction has been shown experimentally to be slow

($k_{aq} = 2 \times 10^6$ dm^{-3} mol^{-1} s^{-1} [2]). Thus, $NH_2^\bullet$ recombination (reaction 23)

$$2NH_2^\bullet = H_2NNH_2 \qquad (23)$$

may compete with it and reform H_2NNH_2 (**1**). This could be a factor contributing to the fact that $G(-H_2NNH_3^+)$ in irradiated solutions is quite low.[2] Another conceivable factor might be the disproportionation reaction 24

$$H_3NNH_3^{\bullet+} + H_2NNH_2^{\bullet+} = 2H_2NNH_3^+; \quad \Delta G°(\text{Rxn}) = -158 \text{ kJ mol}^{-1} \qquad (24)$$

which regenerates $H_2NNH_3^+$. However, that requires the half-life of $H_3NNH_3^{\bullet+}$ (**6**) with respect to $NH_2^\bullet$ formation to be in the $10^{-5}-10^{-4}$ s time scale, which seems unlikely from the present findings.

Concluding Remarks

This study has provided thermochemical results which facilitate the development of mechanisms for the reactions of $OH^\bullet$ and $H^\bullet$ with hydrazine. In the gas phase, barrier heights above reactants are generally low for the H abstraction reactions of both $OH^\bullet$ (-5 kJ mol^{-1}) and $H^\bullet$ (25 kJ mol^{-1}) with H_2NNH_2 (**1**). These findings are consistent with the low activation energies observed experimentally. With $OH^\bullet$ in the gas phase both H_2NNH_2 (**1**) and $H_2NNH_3^+$ (**2**) exhibit evidence for the formation of prereaction complexes, and as a result those reactions may exhibit negative activation energies. That is particularly true for $H_2NNH_3^+$ (**2**), where a strong ion−dipole interaction is involved.

Reaction profiles for attack at both the H_2N and NH_3^+ sites were examined in the case of $H_2NNH_3^+$ (**2**). For $OH^\bullet$ in the gas phase, abstraction of H from the NH_3^+ end to form $H_2NNH_2^{\bullet+}$ (**4**) is preferred over production of $HNNH_3^{\bullet+}$ (**5**) by attack at H_2N. However, probably because of preferred water bonding to the NH_3^+ end, both centers are observed to be attacked in solution. The $\Delta_f G°$(aq) values in Table 2 show that $H_2NNH_2^{\bullet+}$ (**4**) is 100 kJ mol^{-1} more stable than $HNNH_3^{\bullet+}$ (**5**), and this explains the rearrangement which has been observed experimentally in solution.

For $H^\bullet$ attack on $H_2NNH_3^+$ (**2**) the formation of $H_2NNH_2^{\bullet+}$ (**4**) has a very low gas phase E_a. However, in solution solvation effects will again interfere, in this case making production of $H_3NNH_3^{\bullet+}$ (**6**) a competitive process. In aqueous solution **6** is expected to be stable toward dissociation to $H^\bullet + H_2NNH_3^+$ (**2**) ($\Delta G°$(react) = +178 kJ mol^{-1}) and toward $H_3N + NH_3^{\bullet+}$ ($\Delta G°$(react) = +27 kJ mol^{-1}). However, it should decompose to $H_2N^\bullet + NH_4^+$ ($\Delta G°$(react) = −13 kJ mol^{-1}), which is in keeping with recent observations. Complexation of water with $H_3NNH_3^{\bullet+}$ (**6**) was shown to lower the barrier height for that rearrangement, but the lifetime with respect to that process remains uncertain.

Acknowledgment. The financial support of the Natural Sciences and Engineering Research Council of Canada is gratefully acknowledged. Generous assistance from Silicon Graphics Corporation with computing facilities is also recognized.

Supporting Information Available: Table of ZPEs and total energies for all species in this study (1 page). Ordering information is given on any current masthead page.

References and Notes

(1) Swaddle, T. W. *Applied Inorganic Chemistry*; University of Calgary Press: Calgary, Canada, 1990; p 231.
(2) Buxton, G. V.; Stuart, C. R. *J. Chem., Soc. Faraday Trans.* **1996**, *92*, 1519. G. V. Buxton, private communication.
(3) Wagman, D. D.; Evans, W. H.; Parker, V. B.; Schumm, R. H.; Halow, I.; Bailey, S. M.; Churney, K. L.; Nuttal, R. L. *J. Phys. Chem. Ref. Data* **1982**, *11*, Suppl. No. 2.
(4) Cotton, F. A.; Wilkinson, G. *Advanced Inorganic Chemistry*; Wiley Interscience: New York, 1988; p 316.
(5) Buxton, G. V. *Radiation Chemistry of the Liquid State: (1) Water and Homogeneous Aqueous Solutions in Radiation Chemistry: Principles and Applications*; Farhartaziz, Rodgers, M. A., Eds.; VCH Publishers: New York, 1987.
(6) Dewhurst, H. A.; Burton, M. *J. Am. Chem. Soc.* **1955**, *77*, 5781.
(7) Belloni, J.; Haissinsky, M. *Int. J. Radiat. Phys. Chem.* **1969**, *1*, 519.
(8) Lefort, M.; Haissinsky, M. *J. Chim. Phys.* **1956**, *53*, 527.
(9) Hayon, E.; Simic, M. *J. Am. Chem. Soc.* **1972**, *94*, 42.
(10) Mezyk, S. P.; Tateishi, M.; MacFarlane, R.; Bartels, D. M. *J. Chem. Soc., Faraday Trans.* **1996**, *92*, 2541.
(11) Ganghi, N.; Wyatt, J. L.; Symons, M. C. R. *J. Chem. Soc., Chem. Commun.* **1986**, 1424.
(12) Frisch, M. J.; Trucks, G. W.; Schlegel, H. B.; Gill, P. M. W.; Johnson, B. G.; Robb, M. A.; Cheeseman, J. R.; Keith, T. A.; Petersson, G. A.; Montgomery, J. A.; Raghavachari, K.; Al-Laham, M. A.; Zakrewski, V. G.; Ortiz, J. V.; Foresman, J. B.; Cioslowski, J.; Stefanov, B. B.; Nanayakkara, A.; Challacombe, M.; Peng, C. Y.; Ayala, P. Y.; Chen, W.; Wong, M. W.; Andres, J. L.; Replogle, E. S.; Gomperts, R.; Martin, R. L.; Fox, D. J.; Binkley, J. S.; Defrees, D. J.; Baker, J.; Stewart, J. P.; Head-Gordon, M.; Gonzalez, C.; Pople, J. A. *Gaussian 94, (SGI-Revision B.3)*; Gaussian, Inc.: Pittsburgh, PA, 1995.
(13) Curtiss, L. A.; Raghavachari, K.; Pople, J. A. *J. Chem. Phys.* **1993**, *98*, 1293.
(14) Del Bene, J. E.; Person, W. B.; Szczepaniak, K. *J. Phys. Chem.* **1995**, *99*, 10705.
(15) The uniform scale factor of 0.95 for thermodynamic calculations was adopted. After this paper had been submitted, it was shown (Scott, A. P.; Radom, L. *J. Phys. Chem.* **1996**, *100*, 16502) that the use of different scale factors are appropriate in different parts of the calculation and that these factors fall in the range 0.96−1.00 for the B3LYP/6-31G(D) procedure. No factors are available for our B3LYP/6-31+G(D,P) procedure.
(16) McQuarrie, D. A. *Statistical thermodynamics*, Harper & Row: New York, 1973.
(17) Nicolaides, A.; Rauk, A.; Glukhovtsev, M. N.; Radom, L. *J. Phys. Chem.* **1996**, *100*, 17460.
(18) Hehre, W. J.; Ditchfield, R.; Radom, L.; Pople, J. A. *J. Am. Chem. Soc.* **1970**, *92*, 4796.
(19) Leroy, G.; Sana, M.; Wilante, C. *J. Mol. Struct.* **1991**, *228*, 37.
(20) Szulejko, J. E.; McMahon, T. B. *J. Am. Chem. Soc.* **1993**, *115*, 7839.
(21) Berkowitz, J.; Ellison, G. B.; Gutman, D. *J. Phys. Chem.* **1994**, *98*, 2744.
(22) Lias, S. G.; Bartmess, J. E.; Liebman, J. F.; Holmes, J. L.; Levin, R. D.; Mallard, W. G. Gas Phase Ion and Neutral Thermochemistry. *J. Phys. Chem. Ref. Data* **1988**, *17*, Suppl. No. 1.
(23) Ma, B.; Lii, J.-H.; Chen, K.; Allingrer, N. L. *J. Phys. Chem.* **1996**, *100*, 11297.
(24) Schlegel, H. B.; Skancke, A. *J. Am. Chem. Soc.* **1993**, *115*, 7465.
(25) Kohata, K.; Fukuyama, T.; Kuchitsu, K. *J. Phys. Chem.* **1982**, *86*, 602.
(26) Gill, P. M. W.; Radom, L. *J. Am. Chem. Soc.* **1988**, *110*, 4931.
(27) Reiser, G.; Habenicht, W.; Muller-Dethlefs, K. *J. Chem. Phys.* **1993**, *98*, 8462.
(28) (a) Ruscic, B.; Berkowitz, J. *J. Chem. Phys.* **1991**, *95*, 4378. (b) Gibson, S. T.; Greene, J. P.; Berkowitz, J. *J. Chem. Phys.* **1985**, *83*, 4319.
(29) Conway, B. E. *Ionic Hydration in Chemistry and Biophysics*; Elsevier: New York, 1981.
(30) Bartmess, J. E. *J. Chem. Phys.* **1994**, *98*, 6240.
(31) Pople, J. A.; Curtiss, L. A. *J. Chem. Phys.* **1991**, *95*, 4385.
(32) Langhoff, S.; Bauschlicher, C. W., Jr.; Taylor, P. R. *Chem. Phys. Lett.* **1991**, *180*, 88.
(33) Chen, Y.; Rauk, A.; Tschuikow-Roux, E. *J. Phys. Chem.* **1991**, *95*, 9900 and references therein.
(34) Yu, D.; Rauk, A.; Armstrong, D. A. *Can. J. Chem.* **1994**, *72*, 471.
(35) Vaghjiani, G. L. *Int. J. Chem. Kinet.* **1995**, *27*, 777.
(36) Frost, A. A.; Pearson, R. G. *Kinetics and Mechanism*; John Wiley & Sons: New York, 1958; p 92.
(37) (a) Wigner, E. P. *Z. Phys. Chem. Abs. B* **1932**, *19*, 203. (b) Johnson, H. S. *Gas-Phase Reaction Rate Theory*; Ronald Press: New York, 1966; pp 133−136. (c) Garrett, B. C.; Truhlar, D. G. *J. Phys. Chem.* **1979**, *83*, 200.
(38) Payzant, J. D.; Cunningham, A. J.; Kebarle, P. *Can. J. Chem.* **1993**, *71*, 1368. M. Meot-Ner, *J. Am. Chem. Soc.* **1984**, *106*, 1265.
(39) Yu, D.; Rauk, A.; Armstrong, D. A. *Can. J. Chem.* **1993**, *71*, 1368.
(40) Roduner, E.; Bartels, D. M. *Ber. Bunsen-Ges. Phys. Chem.* **1992**, *96*, 1037.
(41) Stanbury, D. M. *Adv. Inorg. Chem.* **1989**, *33*, 69.